CHEMISTRY
A EUROPEAN JOURNAL

DOI: 10.1002/chem.201000764

# Pentiptycene-Derived Light-Driven Molecular Brakes: Substituent Effects of the Brake Component

**Wei-Ting Sun,[a] Yau-Ting Huang,[a] Guan-Jhih Huang,[a] Hsiu-Feng Lu,[b] Ito Chao,*[b] Shou-Ling Huang,[a] Shing-Jong Huang,[a] Ying-Chih Lin,[a] Jinn-Hsuan Ho,[a, c] and Jye-Shane Yang*[a]**

**Abstract:** Five pentiptycene-derived stilbene systems (**1R**; **R** = H, OM, NO, Pr, and Bu) have been prepared and investigated as light-driven molecular brakes that have different-sized brake components (**1H** < **1OM** < **1NO** < **1Pr** < **1Bu**). At room temperature (298 K), rotation of the pentiptycene rotor is fast ($k_{rot} = 10^8$–$10^9\ s^{-1}$) with little interaction with the brake component in the *trans* form ((*E*)-**1R**), which corresponds to the brake-off state. When the brake is turned on by photoisomerization to the *cis* form ((*Z*)-**1R**), the pentiptycene rotation can be arrested on the NMR spectroscopic timescale at temperatures that depend on the brake component. In the cases of (*Z*)-**1NO**, (*Z*)-**1Pr**, and (*Z*)-**1Bu**, the rotation is nearly blocked ($k_{rot} = 2$–$6\ s^{-1}$) at 298 K. It is also demonstrated that the rotation is slower in [$D_6$]DMSO than in $CD_2Cl_2$. A linear relationship between the free energies of the rotational barrier and the steric parameter *A* values is present only for (*Z*)-**1H**, (*Z*)-**1OM**, and (*Z*)-**1NO**, and it levels off on going from (*Z*)-**1NO** to (*Z*)-**1Pr** and (*Z*)-**1Bu**. DFT calculations provide insights into the substituent effects in the rotational ground and transition states. The molar reversibility of the *E*–*Z* photoswitching is up to 46%, and both the *E* and *Z* isomers are stable under the irradiation conditions.

**Keywords:** conformation analysis · fused-ring systems · isomerization · photochromism · substituent effects

## Introduction

The concept of the "bottom-up approach toward miniature devices" has led to the development of many prototypes of molecule- and supramolecule-based machinery systems[1] that mimic the macroscopic counterparts such as brakes,[2] gears,[3] shuttles,[4] and motors.[5] One of the most important issues in operating a molecular machine is the input of energy (fuel). Whereas biological systems such as adenosine triphosphate (ATP) synthases and myosins use chemical energy,[6] artificial molecular machines can adopt photons and electrons as well as chemicals as their energy sources.[7] In this context, photochemically and electrochemically driven systems are particularly intriguing, because they are free of the problem of accumulation of chemical waste during the operation.[8]

We recently communicated[9] a light-driven molecular brake **1NO** (Figure 1), which displays an unprecedented brake performance: namely, the rotation rate ($k_{rot}$) for the rotor is decreased by nearly 9 orders of magnitude at ambient temperature (298 K) upon switching on the brake. In **1NO**, the paddle-wheel-like pentiptycene group serves as the rotor, the dinitrophenyl group as the brake component, and the vinyl linker as the photocontrollable switch through *trans*–*cis* (*E*–*Z*) isomerization. Whereas the brake unit has negligible noncovalent interactions with the rotor in the *trans* (*E*) form, the interactions in the *cis* (*Z*) form are so significant that rotation of the rotor is nearly inhibited. Thus, the *trans* ((*E*)-**1NO**) and *cis* ((*Z*)-**1NO**) isomers corre-

[a] W.-T. Sun, Y.-T. Huang, G.-J. Huang, S.-L. Huang, Dr. S.-J. Huang, Prof. Y.-C. Lin, Dr. J.-H. Ho, Prof. J.-S. Yang
Department of Chemistry, National Taiwan University
Taipei 10617 (Taiwan)
Fax: (+886) 223636359
E-mail: jsyang@ntu.edu.tw

[b] Dr. H.-F. Lu, Prof. I. Chao
Institute of Chemistry, Academia Sinica
Taipei 11529 (Taiwan)
Fax: (+886) 227831237
E-mail: ichao@chem.sinica.edu.tw

[c] Dr. J.-H. Ho
Current address: Department of Chemical Engineering
National Taiwan University of Science and Technology
Taipei 10607 (Taiwan)

Supporting information for this article is available on the WWW under http://dx.doi.org/10.1002/chem.201000764.

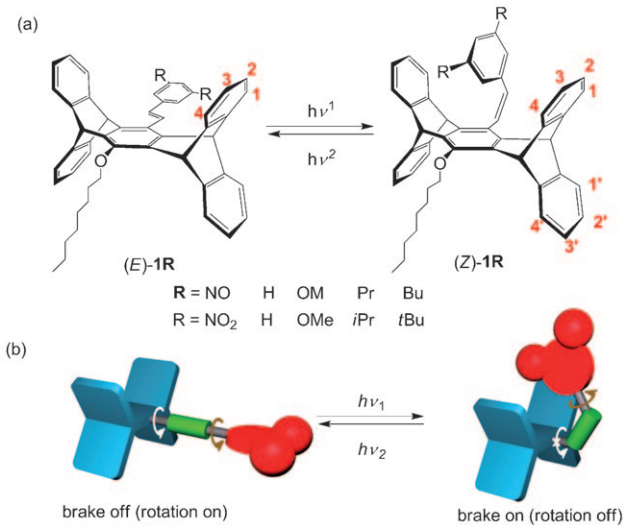


Figure 1. a) Molecular structures and b) schematic illustrations of pentiptycene-derived light-driven molecular brakes (**1R**) that differ in the substituents in the brake component. The *trans* ((*E*)-**1R**) and *cis* ((*Z*)-**1R**) isomers correspond to the brake-off and brake-on states. The numerical labels for protons and carbons are for discussion of the VT NMR spectra. The white and brown curved arrows denote the internal rotation of the rotor and the brake groups, respectively.

spond to the brake-off ($k_{rot}=10^8$–$10^9\ s^{-1}$) and the brake-on ($k_{rot}=3\ s^{-1}$) states, respectively. Because of the $C_2$ symmetry of the pentiptycene rotor, there are two large U-shaped cavities and two shallower V-shaped ones. In the *Z* form, the former can accommodate the brake component, but the latter are inaccessible to the brake component as a result of severe steric interactions with the bridgehead and phenylene hydrogen atoms. Consequently, conformers with the brake component aligned toward the U- and V-shaped cavities correspond to the ground state and the rotational transition state, respectively (Figure 2). Thus, the brake component encounters two isoenergetic ground and transition states during a full turn of the rotor in (*Z*)-**1NO**. We can envisage

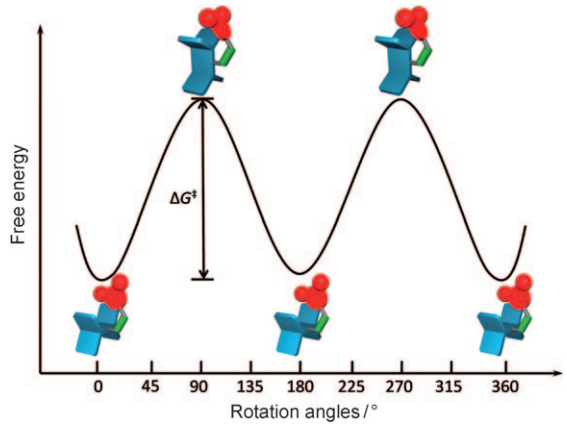


Figure 2. Rotational energy diagram for a full turn of the rotor in (*Z*)-**1R** (the brake-on state). The rotation angle is arbitrarily defined.

that the brake size would play an important role in the torsional barrier of the pentiptycene rotor.

We report herein the synthesis of a series of **1NO** analogues, namely, **1H**, **1OM**, **1Pr**, and **1Bu**, by replacing the nitro groups in the brake component with smaller (H and methoxy) or larger (isopropyl and *tert*-butyl) substituents. In conjunction with **1NO**, the substituent effects on the brake performance could be addressed. Our results show that not only the size but also the electronic nature of the substituents affects the ground and the transitional states of the brake-on from ((*Z*)-**1R**), thus leading to substituent-dependent rotation kinetics for the rotor and the brake. The substituents also affect the quantum efficiency and molar reversibility of *E*--*Z* photoisomerization. The solvent effect on the rotation kinetics is also demonstrated.

## Results and Discussion

**Synthesis**: The stilbene backbone in **1R** (**R**=NO, H, OM, Pr, or Bu) was constructed by either Wittig reaction between the pentiptycene carbaldehyde **2** and the corresponding phosphorus ylides or by Heck reaction with iodopentiptycene **3** and substituted styrenes. The synthesis of both the pentiptycene building blocks **2** and **3** has been reported.[10] Compounds **1NO**, **1H**, and **1OM** were prepared by the Wittig route, and **1Pr** and **1Bu** through the Heck route (Scheme 1), simply depending on the relative ease of synthesis of the desired phosphorus ylides and styrenes. For example, the benzyl chlorides for the Wittig route toward **1NO** and **1OM** could be obtained from the reaction of thionyl chloride and commercially available 3,5-dimethoxybenzyl alcohol (**4**) and 3,5-dinitrobenzyl alcohol (**5**), respectively. The styrenes for the Heck route toward **1Pr** and **1Bu** could be prepared from the corresponding 3,5-dialkyl bromobenzenes by reacting with vinylmagnesium bromide under the catalysis of [Pd(dppf)$Cl_2$] (dppf=1,1′-bis(diphenylphosphino)ferrocene). The starting material 1-bromo-3,5-di(*tert*-butyl)benzene (**6**) is commercially available, and 1-bromo-3,5-diisopropylbenzene (**7**) can be obtained from 2-amino-1,3-diiso-

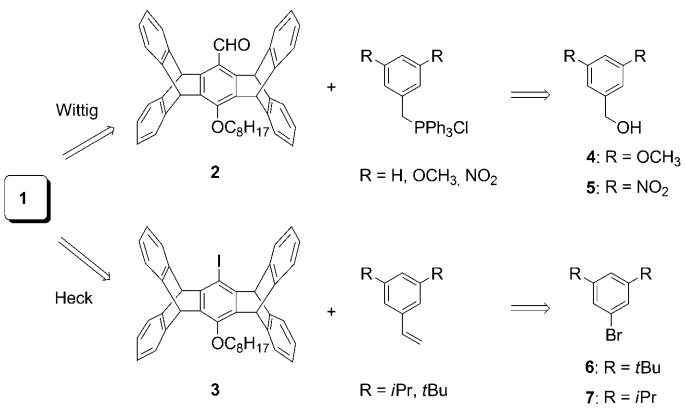


Scheme 1. Retrosynthesis of molecular brakes **1**.

  

propylbenzene by following the literature procedures.[11] It should be noted that the Wittig route gave a mixture of *E* and *Z* isomers, which could be separated by column chromatography (**1NO**) or by preparative high-performance liquid chromatography (HPLC; **1H** and **1OM**). In contrast, the Heck route led to the *E* isomers only. Under the irradiation of 340 nm light, the *E* isomers were converted to the corresponding *Z* isomers with a nearly quantitative yield. See the Experimental Section for detailed synthetic procedures and compound characterization data.

**Variable-temperature (VT) NMR spectroscopy and rotation kinetics**: The two aryl groups (i.e., the rotor and the brake units) of the stilbene backbone in **1R** can undergo independent internal rotation about the aryl–vinyl single bonds (Figure 1b). In the *E* form, the rotational barriers are expected to be low for both the rotor and the brake due to their negligible steric interactions. However, their close proximity in the *Z* form significantly raises their rotational barriers. In principle, the bulkier is the brake unit, the larger is the steric hindrance, and thus a larger rotational barrier for the rotor is expected. On the basis of the steric parameter *A* values (in kcal mol$^{-1}$),[12] the relative size of the brake unit in **1R** increases in the order **1H** ($A=0$) < **1OM** ($A=0.6$) < **1NO** ($A=1.1$) < **1Pr** ($A=2.2$) < **1Bu** ($A=4.8$).

To investigate the rotation kinetics (barriers and rates) of (*Z*)-**1R**, we have carried out variable-temperature $^1$H and $^{13}$C NMR spectroscopic studies (500 and 125 MHz, respectively) and spectral simulations. The spectra were recorded in $CD_2Cl_2$ for **1H** and **1OM** to observe decoalescence of the signals below room temperature and in [$D_6$]DMSO for **1NO**, **1Pr**, and **1Bu** to reach coalescence of the split signals above room temperature (vide infra). To compare the solvent effect on the rotation kinetics, **1Pr** was also studied in $CD_2Cl_2$. Spectral simulations for retrieving the rotation rate were exerted based on VT $^{13}$C NMR spectra rather than the corresponding $^1$H NMR spectra, because the latter is complicated by the multiplicity of proton signals and the presence of more than one type of spin system in the pentiptycene rotor. In the following, the experimental and simulated NMR spectra will be shown for the two extremes in terms of the brake size, **1H** and **1Bu**, and those for **1OM** and **1Pr** are supplied as Supporting Information. The detailed VT NMR spectra for **1NO** have recently been communicated.[9]

Figure 3 shows the aromatic region of $^1$H and $^{13}$C NMR spectra of (*E*)-**1H**, (*Z*)-**1H**, (*E*)-**1Bu**, and (*Z*)-**1Bu** at 298 K. Except for some quaternary carbon atoms, the signals can be unambiguously assigned on the basis of a series of 2D NMR spectroscopic experiments, including COSY, HSQC, NOESY, and ROESY (see the Supporting Information). The numerical labels in Figure 3 correspond to the labeled protons and carbon atoms in Figure 1. The presence of only one set of signals for both the *E* isomers is, as expected, an indication of fast rotation of both the rotor and the brake units about the $C_{vinyl}$–$C_{aryl}$ single bonds. This is also true for (*E*)-**1OM**, (*E*)-**1NO**, and (*E*)-**1Pr** (see the Supporting Information). Our previous DFT calculations on (*E*)-**1NO** suggest a rotational barrier as low as 4.45 kcal mol$^{-1}$.[9] Regarding the Z isomers, the pentiptycene methine nuclei signals are also of one set for (*Z*)-**1H** but become two sets for (*Z*)-**1Bu**. This suggests that rotation of the pentiptycene rotor in (*Z*)-**1H** and (*Z*)-**1Bu** at 298 K is at a rate that is faster and slower, respectively, than the NMR spectroscopic timescale. The situation with (*Z*)-**1NO** resembles the case of (*Z*)-**1Bu**,[9] but (*Z*)-**1OM** and (*Z*)-**1Pr** lie in between the cases of (*Z*)-**1H** and (*Z*)-**1Bu**: namely, the signals for (*Z*)-**1OM**

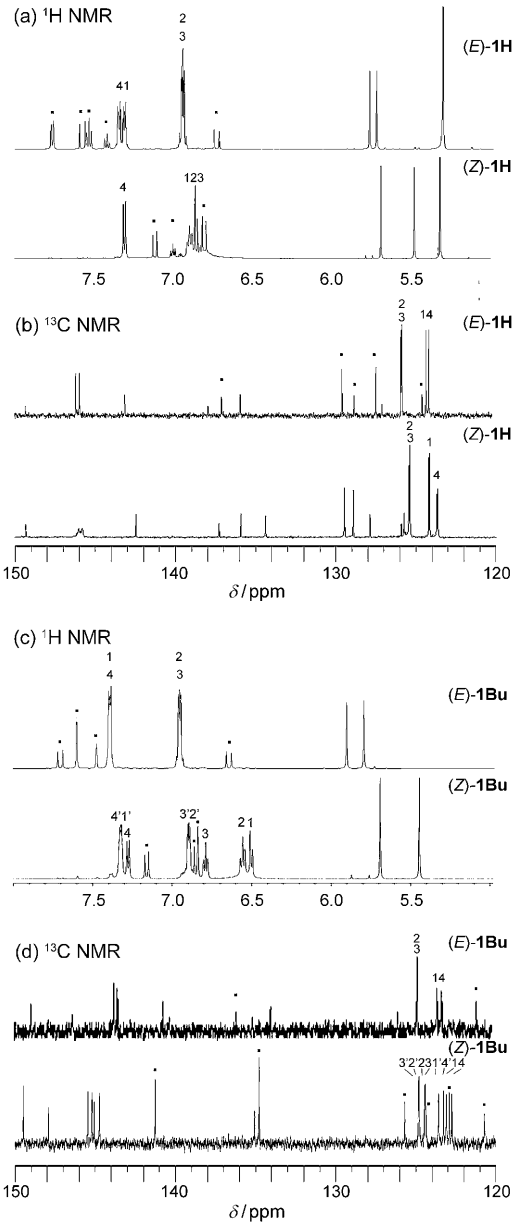


Figure 3. Aromatic region of a) $^1$H and b) $^{13}$C NMR spectra of (*E*)-**1H** and (*Z*)-**1H** in $CD_2Cl_2$, and that of c) $^1$H and d) $^{13}$C NMR spectra of (*E*)-**1Bu** and (*Z*)-**1Bu** in [$D_6$]DMSO at 298 K. The solid circles denote peaks due to the styryl group (the brake and the vinyl switch components), and the Arabic numerals denote the corresponding protons and carbon atoms labeled in Figure 1.

  

and (*Z*)-**1Pr** are broad and unresolved (see the Supporting Information). This arises from the fact that at 298 K the rotation rate for the rotor in (*Z*)-**1OM** and (*Z*)-**1Pr** is approaching the NMR spectroscopic timescale. For the nuclei in the brake unit, there is only one set of signals for all five compounds at 298 K, thereby indicating that the U-shaped cavities of the pentiptycene group provide sufficient space for fast rotation of the brake components. Nevertheless, the rotation rate of the brake unit should also depend on the substituents. We will show below that the rotation of the brake unit could not be arrested on the NMR spectroscopic timescale for all cases, except for the one with the bulky *t*Bu substituents ((*Z*)-**1Bu**), even at temperatures as low as 178 K.

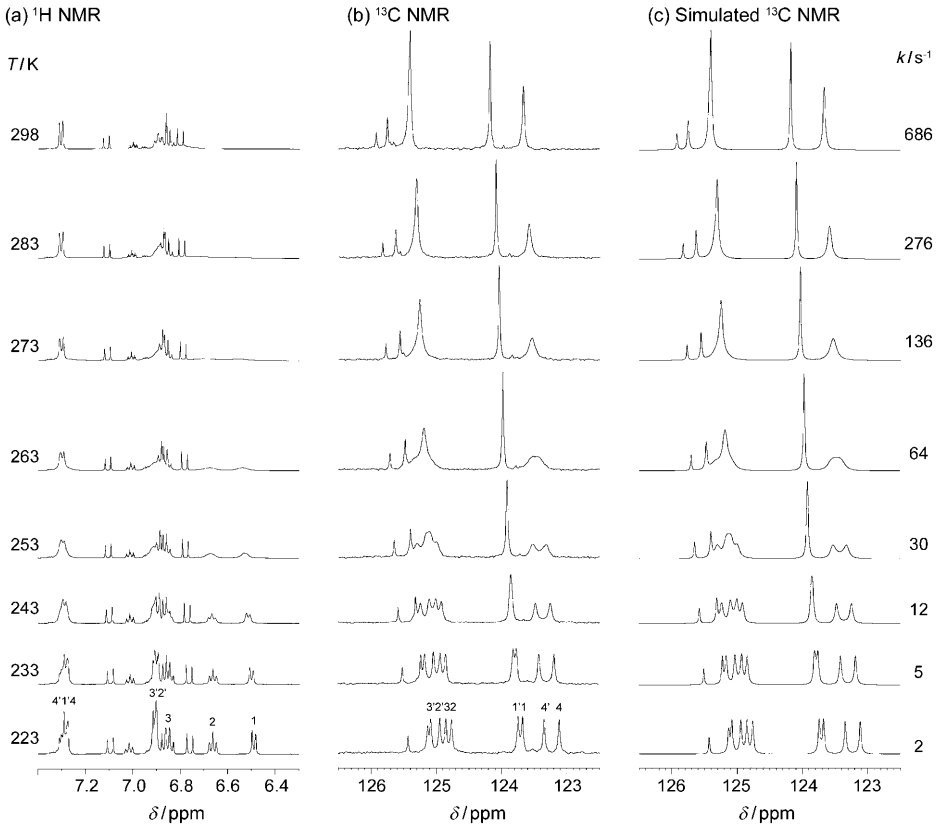


Figure 4. Pentiptycene peripheral phenylene (blade of the rotor) region of the a) experimental proton, b) carbon, and c) simulated carbon VT NMR spectra of (*Z*)-**1H** ($CD_2Cl_2$). Values of temperature (*T* in K) and interconversion rate (*k* in $s^{-1}$) between the two isoenergetic states are also given for every trace.

Figure 4 shows the pentiptycene region of $^1$H and $^{13}$C NMR spectra for (*Z*)-**1H** at different temperatures. The pentiptycene methine signals (those with numerical labels) split into two sets upon cooling from 298 to 223 K, thereby indicating an arrest of the rotation of the pentiptycene rotor on the NMR spectroscopic timescale. The coalescence temperature ($T_c$) for $C_4$ and $C_{4'}$ is near 273 K, which corresponds to an energy barrier of $\Delta G^{\ddagger}_{(273K)} = 13.7$ kcal mol$^{-1}$. On the basis of lineshape simulations (Figure 4c), the rotation is nearly blocked at 223 K, and the rate constant (*k*) for interconversion between the two isoenergetic conformers of (*Z*)-**1H** is only 2 $s^{-1}$. In other words, it takes around 1 s for a 360° rotation of the rotor (i.e., $k_{rot} = k/2$). The activation energy ($E_a$) and pre-exponential factor (log *A*) and enthalpic ($\Delta H^{\ddagger}$) and entropic ($\Delta S^{\ddagger}$) contributions to the free energy of activation ($\Delta G^{\ddagger}$) obtained by Arrhenius and Eyring plots (see the Supporting Information) are reported in Table 1.

Figure 5 shows the pentiptycene region of $^1$H and $^{13}$C NMR spectra for (*Z*)-**1Bu** at different temperatures. Since the rotation of the pentiptycene rotor is slower than the NMR spectroscopic timescale at 298 K, as indicated by the presence of two set of signals for the pentiptycene methine nuclei (Figure 3), it requires a higher temperature to observe coalescence of the signals. Indeed, the peaks of $C_3$ and $C_{3'}$ coalesce upon raising the temperature to 353 K. Like the case of (*Z*)-**1H**, spectral simulations on the VT $^{13}$C NMR spectra (Figure 5c) allow one to retrieve the rate constants *k* and thus $k_{rot}$ for (*Z*)-**1Bu**. The $E_a$, log *A*, $\Delta H^{\ddagger}$, $\Delta S^{\ddagger}$, and $\Delta G^{\ddagger}$ values are reported in Table 1.

Table 1 also summarizes the activation parameters for the rotation of the pentiptycene rotor in (*Z*)-**1OM**, (*Z*)-**1NO**, and (*Z*)-**1Pr**. Since the five compounds of (*Z*)-**1R** differ

Table 1. VT $^{13}$C NMR spectroscopic data and activation parameters for the rotation of the pentiptycene rotor in (*Z*)-**1R**.

| Compound | Solvent | $T_c$[a] [K] | $\Delta G^{\ddagger}_c$ [kcal mol$^{-1}$] | $E_a$ [kcal mol$^{-1}$] | Log *A* | $\Delta H^{\ddagger}$ [kcal mol$^{-1}$] | $\Delta S^{\ddagger}$ [cal mol$^{-1}$ K$^{-1}$] | $\Delta G^{\ddagger}_{(298K)}$ [kcal mol$^{-1}$] | $k_{(298K)}$ [$s^{-1}$] |
|---|---|---|---|---|---|---|---|---|---|
| (*Z*)-**1H** | $CD_2Cl_2$ | 273(4,4′) | 13.7 | 10.5 ± 0.1 | 10.5 ± 0.1 | 10.0 ± 0.1 | −12.1 ± 0.4 | 13.6 ± 0.1 | 686 |
| (*Z*)-**1OM** | $CD_2Cl_2$ | 308(4,4′) | 14.9 | 11.7 ± 0.1 | 10.5 ± 0.1 | 11.1 ± 0.1 | −12.3 ± 0.5 | 14.8 ± 0.2 | 89 |
| (*Z*)-**1NO** | [D$_6$]DMSO | 348(3,3′) | 16.9 | 14.8 ± 0.5 | 11.5 ± 0.2 | 14.1 ± 0.5 | −7.6 ± 1.4 | 16.4 ± 0.5 | 6 |
| (*Z*)-**1Pr** | $CD_2Cl_2$ | – | – | 13.2 ± 0.1 | 10.9 ± 0.1 | 12.6 ± 0.1 | −10.6 ± 0.3 | 15.8 ± 0.1 | 17 |
| | [D$_6$]DMSO | 343(1,1′) | 16.9 | 14.1 ± 0.3 | 11.3 ± 0.2 | 13.5 ± 0.3 | −9.0 ± 0.8 | 16.2 ± 0.3 | 11 |
| (*Z*)-**1Bu** | [D$_6$]DMSO | 353(3,3′) | 17.8 | 14.0 ± 0.8 | 10.8 ± 0.5 | 13.3 ± 0.7 | −11.5 ± 2.3 | 16.8 ± 0.7 | 4 |

[a] Coalescence temperature for protons with labels (see Figure 1) shown in parentheses.

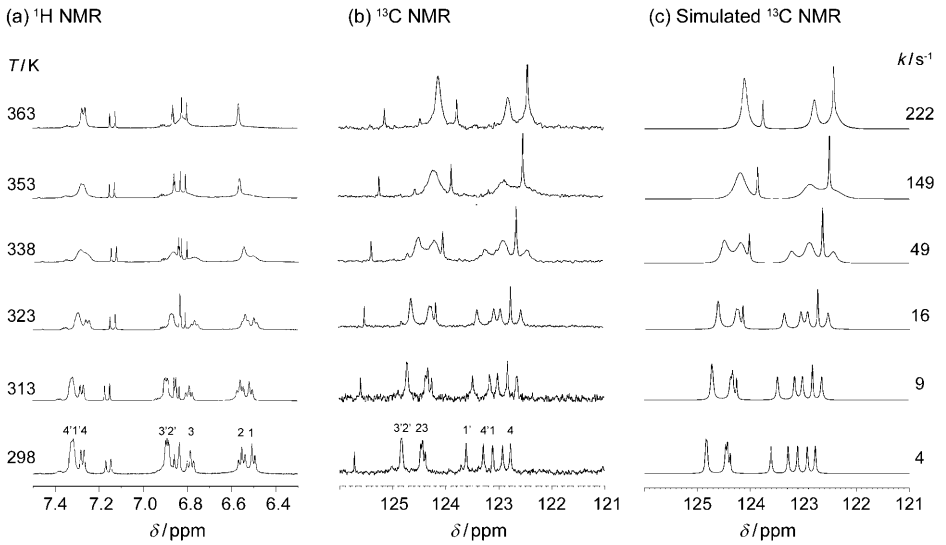


Figure 5. Pentiptycene peripheral phenylene (blade of the rotor) region of the a) experimental proton, b) carbon, and c) simulated carbon VT NMR spectra of (*Z*)-**1Bu** ([$D_6$]DMSO). Values of temperature (*T* in K) and interconversion rate (*k* in $s^{-1}$) between the two isoenergetic states are also given for every trace.

only in the substituents in the brake component (Figure 1a), their differences and similarities in rotation kinetics will reflect the size and electronic effects of the substituents. In this context, we adopt the steric parameter *A* values,[12] defined based on the energy difference (in kcal mol$^{-1}$) between substituted cyclohexane in equatorial versus axial positions, for the discussion of the substituent size effect.

The plot of $\Delta G^{\neq}_{(298K)}$ in [$D_6$]DMSO against the substituent *A* values for (*Z*)-**1R** is shown in Figure 6. Since the experimental $\Delta G^{\neq}_{(298K)}$ values were not determined entirely in the same solvent but either in [$D_6$]DMSO or in $CD_2Cl_2$, we need to consider the influence of solvent on $\Delta G^{\neq}_{(298K)}$ before addressing the substituent effects in (*Z*)-**1R**. The determined $\Delta G^{\neq}_{(298K)}$ value for (*Z*)-**1Pr** in [$D_6$]DMSO is 0.4 kcal mol$^{-1}$ higher than in $CD_2Cl_2$ (Table 1), which is consistent with its higher viscosity ($CH_2Cl_2$: 0.45 MPa s, DMSO: 2.20 MPa s).[13] By the assumption of a similar extent of increase in $\Delta G^{\neq}_{(298K)}$ for (*Z*)-**1H** and (*Z*)-**1OM** on changing the solvent from $CD_2Cl_2$ to [$D_6$]DMSO, their $\Delta G^{\neq}_{(298K)}$ values in [$D_6$]DMSO would be 14.0 and 15.2 kcal mol$^{-1}$, respectively. The absence of a linear relationship in Figure 6 reveals that the substituent effects on the ground versus the transition states of (*Z*)-**1R** are different from those on the equatorial versus axial conformation of cyclohexane. Regarding the π-conjugated nature of (*Z*)-**1R**, the electronic effect of the substituents should also be important in determining the energy of (*Z*)-**1R** in the rotational ground and transition states.

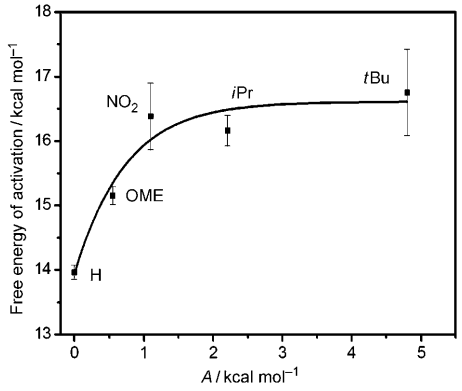


Figure 6. The relationship between the size of substituents (*A* value) on the brake component and the rotational free energy of activation ($\Delta G^{\neq}$) for the rotor of (*Z*)-**1R** in [$D_6$]DMSO at 298 K.

It is interesting to point out that among the five (*Z*)-**1R** species (*Z*)-**1NO** possesses the largest $\Delta H^{\neq}$ value and the smallest $\Delta S^{\neq}$ value (Table 1). One possible explanation is the presence of specific attractive interactions for (*Z*)-**1NO** in the ground state. In view of the polar nature of the nitro groups, it could be attributed to electrostatic interactions between the dinitrophenyl group (the brake component) and the peripheral phenylene rings of pentiptycene (the blades of the rotor). However, such interactions (favorable in enthalpy) require more specific alignments between the phenylene rings (unfavorable in entropy). This phenomenon is reminiscent of the concept of enthalpy–entropy compensation.[14]

The relatively broad $^1$H NMR spectroscopic signals for the *t*Bu groups in (*Z*)-**1Bu** at 298 K prompted us to investigate whether the rotation of the brake unit (denoted by the brown curved arrows in Figure 1b) could be arrested on the NMR spectroscopic timescale at low temperatures. Indeed, on the basis of the VT $^1$H NMR spectra in $CD_2Cl_2$ and the simulated spectra (Figure 7), the interconversion rate constant (*k*) between the two isoenergetic states is as low as 12 $s^{-1}$ at 178 K. The coalescence temperature ($T_c$) for the two *t*Bu groups is near 238 K, which corresponds to a $\Delta G^{\neq}_c$ value of 10.7 kcal mol$^{-1}$. The $E_a$ and $\Delta H^{\neq}$ values are (7.0 ± 0.1) and (6.7 ± 0.1) kcal mol$^{-1}$, respectively, both of which are only one-half the size for the pentiptycene rotation (14.0 and 13.3 kcal mol$^{-1}$, Table 1). However, the entropic term ($\Delta S^{\neq} = (-15.3 \pm 0.3)$ cal K$^{-1}$ mol$^{-1}$) that contributes to the rotational barrier is considerably larger than the cases of the pentiptycene rotation (Table 1). This corresponds to a low log *A* value (9.7 ± 0.1). Consequently, the free energy of activation at 298 K ($\Delta G^{\neq}_{(298K)}$) is significant (11.2 kcal mol$^{-1}$).

**Computational study**: To gain further insight into the substituent effects on the ground and the transition states of

  

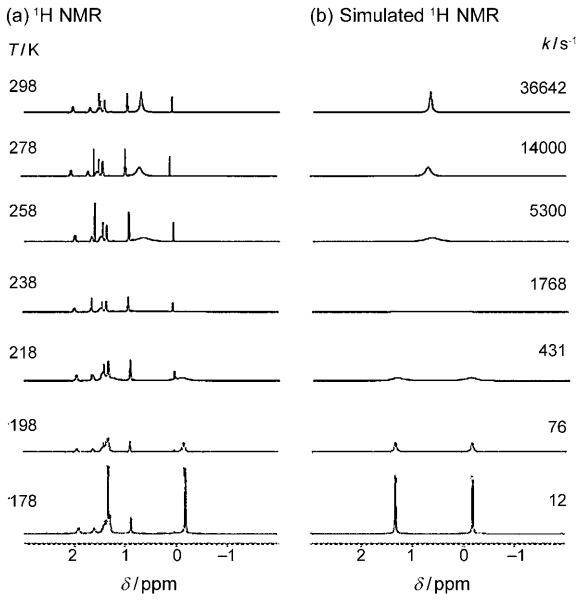


Figure 7. The upfield region $\delta = -2$–3 ppm of the a) experimental and b) simulated VT $^1$H NMR spectra of (*Z*)-**1Bu** ($CD_2Cl_2$, 500 MHz). Values of temperature ($T$ in K) and interconversion rate ($k$ in $s^{-1}$) between the two isoenergetic states are also given for every trace.

(*Z*)-**1R**, we have carried out DFT calculations. In the previous communication,[9] we reported that at the BMK/6-311+G**//B3LYP/6-31G* theory level[15] the calculated $\Delta G^{\neq}_{(298K)}$ value for the rotor ($\Delta G^{\neq}_{(298K)}$(rotor) = 16.75 kcal mol$^{-1}$) for (*Z*)-**1NO** agrees well with the experimental value (16.4 kcal mol$^{-1}$ in [$D_6$]DMSO) even though solvation was not considered in the calculations. Thus, the same theory level was adopted for the calculation of the other (*Z*)-**1R** compounds. As in the previous study, the octyloxy group *para* to the brake unit was replaced by a methoxy group to expedite the calculations. What is different from the previous study is that the rotation barriers are estimated on the basis of free energies of multiple conformers with the consideration of Boltzmann distribution, rather than the lowest-energy structures of the ground and transition states.[16] The difference between the DFT-derived $\Delta G^{\neq}_{(298K)}$(rotor) values (Table 2) and the observed data (Table 1) is 1.32 kcal mol$^{-1}$ for (*Z*)-**1H** and smaller for the other (*Z*)-**1R** species. It is noted that the Boltzmann distribution treatment narrows the difference (from 0.35 to 0.19 kcal mol$^{-1}$) between the calculated and experimental $\Delta G^{\neq}_{(298K)}$(rotor) values for (*Z*)-**1NO**. Although the substituent dependence of the calculated $\Delta G^{\neq}_{(298K)}$(rotor) is less prominent than that of the experimental values, the order (*Z*)-**1H** < (*Z*)-**1OM** < (*Z*)-**1Pr** < (*Z*)-**1Bu** is consistent with the observed trend. The calculated $\Delta G^{\neq}_{(298K)}$(rotor) of (*Z*)-**1NO** is close to that of (*Z*)-**1Bu**, similar to what is observed experimentally, but the order is reversed. Overall, both experimental and DFT results show that $\Delta G^{\neq}_{(298K)}$(rotor) does not correlate linearly with the substituent $A$ value.

Table 2. DFT-derived rotational barriers and homodesmotic reaction free energy[a] for (*Z*)-**1R** in the ground and transition states along the rotor and the brake rotation coordinates at 298 K.

| Compound | $\Delta G_{hom}$(G)[b] | $\Delta G_{hom}$(T)[c] | | $\Delta\Delta G^{\neq}$[d] | | $\Delta G^{\neq}_{(298K)}$[e] | |
|---|---|---|---|---|---|---|---|
| | | rotor | brake | rotor | brake | rotor | brake |
| (*Z*)-**1H** | 0.00 | 0.00 | 0.00 | 0.00 | 0.00 | 14.92 | 6.77 |
| (*Z*)-**1OM** | 1.02 | 1.25 | 2.89 | 0.23 | 1.87 | 15.15 | 8.63 |
| (*Z*)-**1NO** | 0.29 | 1.96 | 0.33 | 1.67 | 0.04 | 16.59 | 6.81 |
| (*Z*)-**1Pr** | 2.55 | 2.89 | 3.31 | 0.34 | 0.76 | 15.26 | 7.53 |
| (*Z*)-**1Bu** | 2.46 | 3.64 | 6.26 | 1.18 | 3.80 | 16.10 | 10.57 |

[a] In kcal mol$^{-1}$ calculated at the BMK/6-311+G**//B3LYP/6-31G* theory level. [b] The (*Z*)-**1H** and (*Z*)-**1R** in Scheme 2 are in the ground state. [c] The (*Z*)-**1H** and (*Z*)-**1R** in Scheme 2 are in the transition state. [d] $\Delta\Delta G^{\neq} = \Delta G_{hom}(T) - \Delta G_{hom}(G)$. [e] The free energy of the rotational barrier at 298 K.

Figure 8 shows the DFT-calculated ground- and transition-state lowest-energy conformations of (*Z*)-**1NO** and (*Z*)-**1Bu** along the rotor rotation coordinate (Figure 2). In the ground states, the brake component is located in the U-shaped cavities with the brake phenylene group tilted toward one of the rotor phenylene rings. As the *t*Bu group is bulkier than the $NO_2$ group, the extent of tilting is less in (*Z*)-**1Bu** than (*Z*)-**1NO** in the lowest-energy structures. In the transition states, the brake phenylene ring is perpendicular to the rotor central phenylene ring and oriented above the V-shaped cavities of the rotor. The steric interactions between the brake phenylene ring and the bridgehead hydrogen atoms of the rotor are significant, as indicated by the short distances between the ring center and the Hs and by the increased aryl–vinyl bond angles on going from the ground state (ca. 130°) to the transition state (ca. 140°). The substituent effect is also manifested in the transition state by the comparison of (*Z*)-**1NO** to (*Z*)-**1Bu**, in which the atom-to-ring (i.e., $H_{bridgehead}$–$Ph_{brake}$) distance is somewhat larger in (*Z*)-**1Bu** (2.80 Å) than (*Z*)-**1NO** (2.73 Å).

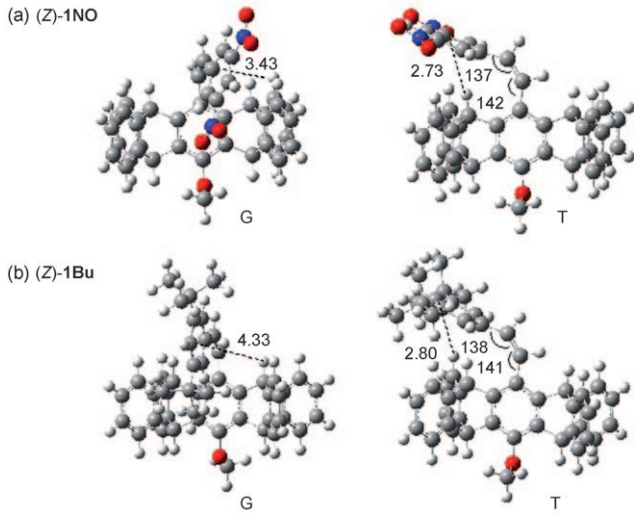


Figure 8. DFT-derived lowest-energy structures for the ground (G) and transition (T) states of a) (*Z*)-**1NO** and b) (*Z*)-**1Bu** along the pentiptycene rotation coordinate. Select distances [Å] and angles [°] are shown.

The relative substituent effect on the ground versus the transition states can be evaluated by homodesmotic reac-

  

tions shown in Scheme 2, in which $\Delta G_{hom}$ is the free energy of (*Z*)-**1R** (disubstituted (*Z*)-**1H**) and benzene relative to (*Z*)-**1H** and *meta*-disubstituted benzene (*m*-**R**). When both

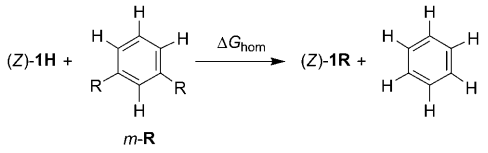


R = OMe (**OM**), $NO_2$ (**NO**), *i*Pr (**Pr**), or *t*Bu (**Bu**)

Scheme 2. The homodesmotic reaction employed to estimate the influence of the brake substituents on the stability of the ground and the transition states of (*Z*)-**1R**.

(*Z*)-**1H** and (*Z*)-**1R** are in the ground state, the $\Delta G_{hom}$ values, denoted as $\Delta G_{hom}$(G), allow one to compare the relative stability of (*Z*)-**1R** in their ground states. Likewise, the corresponding $\Delta G_{hom}$ values in the transition states of the rotor rotation, denoted as $\Delta G_{hom}$(T)(rotor), reveal the relative stability of (*Z*)-**1R** in their transition states along the rotor rotation coordinate (Figure 2). As summarized in Table 2, both the $\Delta G_{hom}$(G) and $\Delta G_{hom}$(T) rotor values are positive. Evidently, the substituents destabilize not only the transition state but also the ground state. It is interesting to note that the $\Delta G_{hom}$(T) rotor value increases monotonically with increasing size of the substituents in the brake component, but no explicit order is present for the $\Delta G_{hom}$(G) values. The $\Delta G_{hom}$(G) value for (*Z*)-**1NO** is relatively small. It is possible that the strong dipole of the nitro substituents lowers the energy of (*Z*)-**1NO** by interacting with the peripheral phenylene rings of pentiptycene,[17] which compensates for the steric repulsion. This is consistent with the argument based on the $\Delta H^{\neq}$ and $\Delta S^{\neq}$ values determined by NMR spectroscopy (vide supra, Table 1). As a result of the comparable substituent effects on the ground and the transition states (i.e., $\Delta\Delta G^{\neq}$(rotor) = $\Delta G_{hom}$(T)-(rotor) − $\Delta G_{hom}$(G) = 0.23–1.67 kcal mol$^{-1}$), the substituent effects on the rotational barriers of (*Z*)-**1R** are smaller than predicted on the basis of the *A* values.

We have also calculated the rotational barriers and homodesmotic reaction free energy for the brake rotation of (*Z*)-**1R** at 298 K (Table 2), since the experimental value of $\Delta G^{\neq}_{(298K)}$(brake) for (*Z*)-**1Bu** is available for comparison. A good agreement between the $\Delta G^{\neq}_{(298K)}$ brake data derived by DFT (10.57 kcal mol$^{-1}$) and determined by NMR spectroscopy (11.2 kcal mol$^{-1}$) is again observed. The difference in the brake rotational barrier between (*Z*)-**1H**, (*Z*)-**1OM**, (*Z*)-**1Pr**, and (*Z*)-**1Bu** suggests that the brake rotation is also dependent of the substituents. The similar rotational barriers calculated for (*Z*)-**1NO** and (*Z*)-**1H** show that the nitro substituents affect the ground and the transition states to a similar extent ($\Delta\Delta G^{\neq}$(brake) = 0.04 for (*Z*)-**1NO** in Table 2). Indeed, as shown in Figure 9a, the transition state of (*Z*)-**1NO** corresponds to a perpendicular orientation of the brake phenylene ring with respect to the pentiptycene

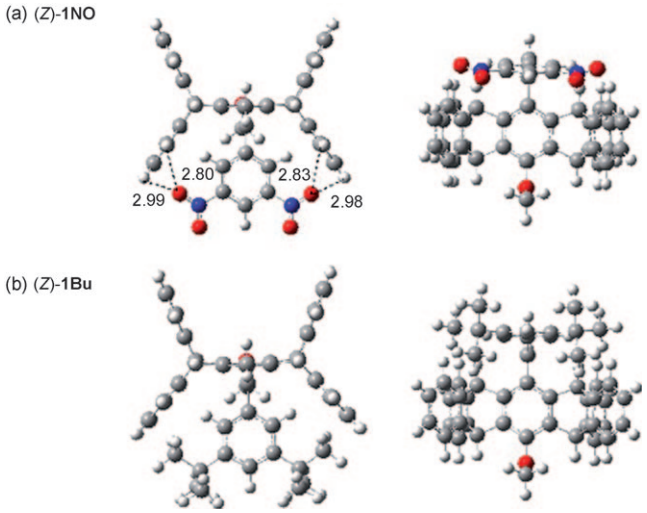


Figure 9. DFT-derived transition-state structures (top and side views) for a) (*Z*)-**1NO** and b) (*Z*)-**1Bu** along the brake rotation coordinate. Select distances [Å] are shown.

phenylene rings on the side of the U-shaped cavities, at which C−H···O interactions are present.

Therefore, despite the larger size of $NO_2$ versus H, these $NO_2$-related attractive interactions counterbalance the increased steric congestion in (*Z*)-**1NO** versus (*Z*)-**1H** in both the ground and transition states, which corresponds to the relatively small $\Delta G_{hom}$(G) and $\Delta G_{hom}$(T) brake values (0.29 and 0.33 kcal mol$^{-1}$, respectively) for (*Z*)-**1NO**. In contrast, the large $\Delta G_{hom}$(T) brake value (2.89 kcal mol$^{-1}$) for (*Z*)-**1OM** indicates that the polar methoxy groups do not induce any explicit attractive interactions with the rotor blades in the transition state. This is also true for the nonpolar substituents *i*Pr and *t*Bu (Figure 9b). It is interesting to note that the $\Delta G_{hom}$(T) brake values for those of nonpolar substituents (i.e., (*Z*)-**1H**, (*Z*)-**1Pr**, and (*Z*)-**1Bu**) correlate well (slope = 1.34, $R^2$ = 0.99) with the substituent *A* values (see the Supporting Information).

Despite the independent internal rotation coordinates for the rotor and the brake units, the strong steric and/or electronic interactions between the two units in (*Z*)-**1R** suggest that their rotations are far from completely independent. For example, formation of the transition states from the ground states along the rotor rotation coordinate (e.g., (*Z*)-**1NO** in Figure 8a) requires the rotation of not only the rotor but also the brake unit (Figure 2). Thus, the rotation dynamics of the brake would affect that of the rotor. An animated view of these processes has been supplied as Supporting Information.

**Photoisomerization**: The photochemical switching between the brake-off ((*E*)-**1R**) and brake-on ((*Z*)-**1R**) states was conducted in $CH_2Cl_2$. The molar ratio of (*E*)-**1R** to (*Z*)-**1R** ([*E*]/[*Z*]) in photostationary states (PSS) depends on the quantum yields for (*E*)-**1R**→(*Z*)-**1R** ($\Phi_{EZ}$) and (*Z*)-**1R**→(*E*)-**1R** ($\Phi_{ZE}$) and on the molar absorptivity of (*E*)-**1R** ($\varepsilon_E$)

and (*Z*)-**1R** ($\varepsilon_Z$) at the excitation wavelengths ($\lambda_{ex}$) according to Equation (1):[18]

$$[E]/[Z] = (\varepsilon_Z \Phi_{ZE})/(\varepsilon_E \Phi_{EZ}) \quad (1)$$

Generally, the values of $\Phi_{EZ}$ and $\Phi_{ZE}$ are independent of $\lambda_{ex}$ based on the Kasha–Valivov rule.[19] Thus, control of the isomer distribution $[E]/[Z]$ mainly relies on the $\varepsilon_E/\varepsilon_Z$ ratio. To achieve the maximum forward and reversed conversion of (*E*)-**1R**→(*Z*)-**1R** and (*Z*)-**1R**→(*E*)-**1R**, the solutions were excited at wavelengths of the maximum and the minimum ratio of $\varepsilon_E/\varepsilon_Z$, respectively. The absorption spectra of both isomers of **1H** are shown in Figure 10 and those of **1NO** are in Figure 11. The absorption spectra of **1OM**, **1Pr**, and **1Bu** resemble those of **1H**, with the maximum and minimum $\varepsilon_E/\varepsilon_Z$ values near 340 and 250 nm, respectively. In these cases, the molar absorptivity of the *Z* isomers is low or negligible at 340 nm, and thus the *Z* isomer is predominant (>98%) in PSS with 340 nm irradiation (Table 3). The molar reversibility (*R*) upon irradiation at 250 nm is 46% for **1Pr** and **1Bu** and slightly lower for **1H** and **1OM**. The absorption spectra of **1NO** differ from the others by shifting the peak maxima toward the shorter wavelengths and by extending the long-wavelength shoulders toward longer wavelengths. This could be attributed to the strong electron-withdrawing nitro groups that lead to a stronger donor–acceptor (charge-transfer) electronic character. As a result of the reduced ratio $\varepsilon_E/\varepsilon_Z$ even at the long-wavelength tail (400 nm), the efficiency for (*E*)-**1NO**→(*Z*)-**1NO** switching is significantly lower than the other species. This in turn leads to a low switching capacity of $R = 20\%$. The isomerization quantum yields and the $[E]/[Z]$ values in PSS are reported in Table 3. These values are consistent with Equation (1) within experimental errors (ca. 10%).

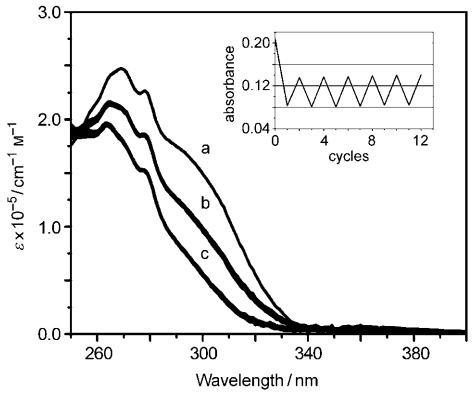


Figure 10. Absorption spectra of (*E*)-**1H** (curve a) and (*Z*)-**1H** (curve c) and their photostationary states irradiated with alternating 340 (curves c) and 250 nm (curves b) UV-light irradiation in dichloromethane. Inset shows the changes in absorbance at 298 nm starting from (*E*)-**1H** (19 μM) for 6 switching cycles.

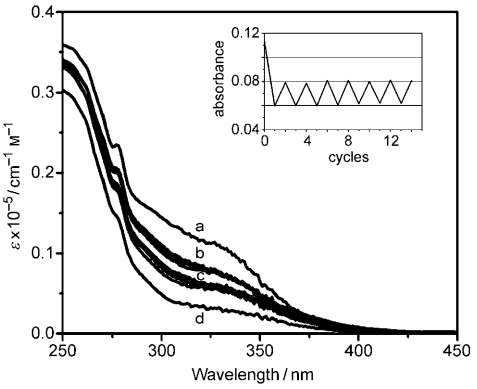


Figure 11. Absorption spectra of (*E*)-**1NO** (curve a) and (*Z*)-**1NO** (curve d) and their photostationary states irradiated with alternating 250 (curves b) and 400 nm (curves c) UV-light irradiation in dichloromethane. Inset shows the changes in absorbance at 322 nm starting from (*E*)-**1NO** (19 μM) for 7 switching cycles.

Table 3. Photochemical data for molecular brakes **1R**.[a]

| Compound | $\Phi_{EZ}$[b] | $\Phi_{ZE}$[c] | $[E]/[Z]_{340}$[d] | $[E]/[Z]_{250}$[e] | $R$[f] [%] |
|---|---|---|---|---|---|
| **1H** | 0.48 | 0.37 | 1:99 | 43:57 | 43 |
| **1OM** | 0.39 | 0.28 | 2:98 | 41:59 | 39 |
| **1NO** | 0.17 | 0.21 | 25:75[g] | 45:55 | 20 |
| **1Pr** | n.d.[h] | n.d.[h] | 1:99 | 46:54 | 46 |
| **1Bu** | 0.49 | 0.38 | 1:99 | 46:54 | 46 |

[a] In $CH_2Cl_2$. [b] Quantum yields for (*E*)-**1R**→(*Z*)-**1R** photoisomerization. [c] Quantum yields for (*Z*)-**1R**→(*E*)-**1R** photoisomerization. [d] Isomer ratio ($[E]/[Z]$) in PSS at $\lambda_{ex} = 340$ nm. [e] Isomer ratio ($[E]/[Z]$) in PSS at $\lambda_{ex} = 250$ nm. [f] Molar reversibility ($\Delta E$ or $\Delta Z$) in PSS with $\lambda_{ex} = 250$ versus 340 nm. [g] $\lambda_{ex} = 400$ nm. [h] n.d. = not determined. The quantum yields of **1Pr** are expected to be similar to that for **1Bu** in view of their similar absorption spectra and isomer distribution in PSS.

To test the photostability of both the *E* and *Z* isomers of **1R**, multiple photoswitching between the two PSS of maximum and minimum $[E]/[Z]$ ratios have been carried out for all five compounds. The results for **1H** and **1NO** are shown in Figures 10 and 11, respectively, and the corresponding data for the others are supplied as Supporting Information. No apparent decomposition was detected after 5–7 switching cycles for all cases, thereby showing that molecular brakes **1R** are quite robust under the operation conditions.

## Conclusion

The pentiptycene-derived stilbenes **1H**, **1OM**, **1NO**, **1Pr**, and **1Bu** display distinct internal rotation rate for the pentiptycene rotor in the *trans* ((*E*)-**1R**) versus the *cis* ((*Z*)-**1R**) forms, which can be reversibly switched by light with an efficiency of 39–46% in molar ratio. At 298 K, the rotation rate in (*E*)-**1** is at a magnitude of $k_{rot} = 10^8$–$10^9\ s^{-1}$ for all five compounds, but it varies from 2 to 686 $s^{-1}$ for (*Z*)-**1R**, depending on the nature of the substituents in the brake component. The substituents exert steric repulsion, electronic induction, and specific attractive electrostatic interactions with the pentiptycene rotor in the ground state as well as the transition state of (*Z*)-**1R** along the rotation coordinate. It is remarkable that DFT calculations provide a nice prediction

  

of the substituents effect on the rotation kinetics. Our results demonstrate not only an efficient and tunable control of the Brownian rotary motion of molecular rotors by photons and small structural variations[20,21] but also the potential utility of the rigid pentiptycene framework[10,22] in constructing molecular machines.

## Experimental Section

**General**: $^1$H (500 MHz) and $^{13}$C (125 MHz) NMR spectra were acquired using a Bruker DMX 500 spectrometer with 5 mm gradient triple-resonance broadband inverse (TBI) and triple-resonance broadband observe (TBO) probes, respectively. The chemical shifts for $^1$H and $^{13}$C spectra were referenced to the signals of tetramethylsilane ($\delta(^1H)=0$ and $\delta(^{13}C)=0$). Single-pulse spectra were recorded using a 30° pulse and a suitable delay time (2 and 6 s for $^1$H and $^{13}$C, respectively). Other spectra (COSY, NOESY, ROESY, and HSQC) were measured using pulse sequences in the Bruker software package. In the case of variable-temperature measurements, the actual sample temperature was well calibrated by $^1$H signals of ethylene glycol and methanol so that the temperature error was assured to be within $\pm 1$ K. Signal acquisition was begun after a sufficient temperature equilibration time (10–15 min). Fitting of dynamic NMR spectroscopic line shapes at different temperatures was performed with the Topspin 2.0 program, Bruker BioSpin Group. Infrared spectra were recorded using a Nicolet Magna-IR 550 Spectrometer Series II. UV/Vis absorption spectra were measured using a Varian Cary300 Biotype at room temperature. Photoswitching experiments were conducted on $N_2$-bubbled solutions ($10^{-5}$ M) at selected wavelengths using a 75 W Xe arc lamp and monochromator. Quantum yields of photoisomerization were measured on optically dense $N_2$-bubbled solutions ($10^{-3}$ M) at 350 nm using a 75 W Xe arc lamp and monochromator. *trans*-4-(Phenylamino)stilbene was used as a reference standard ($\Phi=0.34$ in dichloromethane).[23] The extent of photoisomerization (<10%) was determined using HPLC analysis (Waters 600 Controller and 996 photodiode array detector) without back-reaction corrections. The reproducibility error was <10% of the average. DFT calculations were performed at the BMK/6-311+G**//B3LYP/6-31G* theory level[14] for (*Z*)-**1** in the gas phase with the consideration of Boltzmann distribution of the possible conformations of the substituents. To expedite the DFT calculations, the octyl group in (*Z*)-**1** was replaced by a methyl group for all cases. All the calculations were performed with the Gaussian 03 package.[24]

**Materials**: THF and $CH_2Cl_2$ were dried with sodium metal and $CaH_2$, respectively, and distilled before use. All the other solvents for spectra and isomerization quantum-yield measurements were HPLC grade and used as received. Compounds **2** and **3** were prepared according to the literature procedures.[10] 3,5-Dialkyl styrenes were prepared by palladium-catalyzed cross-coupling reaction of Grignard reagents with dialkylbromobenzene.[25] Synthetic details for compounds (*E*)-**1NO** and (*Z*)-**1NO** have been reported.[9]

**Synthesis of 1-(chloromethyl)-3,5-dimethoxybenzene**: $SOCl_2$ (0.6 mL, 8.3 mmol) was added to a mixture of 3,5-dimethoxybenzyl alcohol (1.0 g, 5.9 mmol), triethylamine (2 mL), and $CH_2Cl_2$ (25 mL) at 0°C. The mixture was then heated to reflux for 3 h. The solution was cooled and concentrated under reduced pressure, and the residue was extracted with $CH_2Cl_2$ and $H_2O$. The organic layer was dried over anhydrous $MgSO_4$, and the filtrate was concentrated under reduced pressure. Flash column chromatography with EA/hexane (v/v=50:50) as the eluent afforded the product with a yield of 86%. M.p. 46–47°C (ref. [26]=46°C); $^1$H NMR (400 MHz, $CDCl_3$): $\delta=3.80$ (s, 6H), 4.52 (t, $J=2.8$ Hz, 2H), 6.41 (d, $J=2.3$ Hz, 1H), 6.54 ppm (s, 2H).

**General procedure for the synthesis of phosphonium halide salts**: A mixture of benzyl chloride (0.5 g, 4.9 mmol), $PPh_3$ (1.4 g, 5.4 mmol), and toluene (5 mL) was heated at reflux for 24 h. The precipitate was filtered off and afforded the salt with a yield over 95%.

**General procedure for the synthesis of 3,5-dialkyl styrenes from 1-bromo-3,5-dialkylbenzene**: Vinylmagnesium bromide (6 mL, 6 mmol) was slowly added to a mixture of 1-bromo-3,5-diialkylbenzene (2 mmol), [Pd(dppf)$Cl_2$] (23 mg, 0.03 mmol), and THF (6 mL) at −78°C under argon. The mixture was kept stirring for 10 min and then heated to reflux for 12 h. The mixture was cooled, 5% $HCl_{(aq)}$ (1 mL) was added, and then extracted with $CH_2Cl_2$. The organic layer was dried over anhydrous $MgSO_4$, and the filtrate was concentrated under reduced pressure. Flash column chromatography with hexane as the eluent afforded the styrene product. 3,5-diisopropylstyrene: yield=75%; $^1$H NMR (400 MHz, $CDCl_3$): $\delta=1.26$ (d, $J=6.9$ Hz, 12H), 2.89 (septet, $J=6.9$ Hz, 2H), 5.21 (dd, $J=10.9$, 1.0 Hz, 1H), 5.74 (dd, $J=17.6$, 1.0 Hz, 1H), 6.72 (dd, $J=17.6$, 10.9 Hz, 1H), 6.99 (t, $J=1.6$ Hz, 1H), 7.10 ppm (d, $J=1.6$ Hz, 2H); $^{13}$C NMR (125 MHz, $CD_2Cl_2$): $\delta=24.0$, 34.2, 113.2, 121.9, 124.5, 137.4, 137.5, 149.1 ppm; HRMS (FAB): *m/z*: calcd for $C_{14}H_{20}$: 188.1565 [$M^+$]; found: 188.1559. 3,5-Di(*tert*-butyl)styrene: yield=84% yield; $^1$H NMR (400 MHz, $CD_2Cl_2$): $\delta=1.35$ (s, 18H), 5.22 (dd, $J=11.2$ Hz, 1.2 Hz, 1H), 5.74 (dd, $J=17.6$ Hz, 1.2 Hz, 1H), 6.75 (dd, $J=17.6$ Hz, 11.2 Hz, 1H), 7.28 (d, $J=1.2$ Hz, 2H), 7.36 ppm (t, $J=1.2$ Hz, 1H).

**General Wittig route for the synthesis of 1R (1H, 1OM, 1NO)**: A mixture of **2** (0.20 g, 0.34 mmol) and benzylphosphonium chloride salts (0.69 mmol), $K_2CO_3$ (0.94 g, 6.81 mmol), and $CH_2Cl_2$ (25 mL) was heated to reflux for 24 h. The solution was cooled and concentrated under reduced pressure, and the residue was dissolved with $CH_2Cl_2$ and $H_2O$. The organic layer was washed with $H_2O$ and then dried over anhydrous $MgSO_4$, and the filtrate was concentrated under reduced pressure. Preparative HPLC with EA/hexane (v/v=5:95) as the eluent afforded the product. (*E*)-**1H**: yield=55%; m.p. 250–251°C; $^1$H NMR (500 MHz, $CD_2Cl_2$): $\delta=0.95$–0.98 (m, 3H), 1.39–1.42 (m, 4H), 1.46–1.56 (m, 4H), 1.71 (m, 2H), 2.05 (tt, $J=6.7$, 7.6 Hz, 2H), 3.96 (t, $J=6.7$ Hz, 2H), 5.73 (s, 2H), 5.78 (s, 2H), 6.74 (d, $J=16.4$ Hz, 1H), 6.92–6.97 (m, 8H), 7.30–7.37 (m, 8H), 7.41–7.44 (m, 1H), 7.52–7.55 (m, 2H), 7.57 (d, $J=16.4$ Hz, 1H), 7.76–7.77 ppm (m, 1H); $^{13}$C NMR (125 MHz, $CD_2Cl_2$): $\delta=14.5$, 23.3, 27.0, 30.0, 30.2, 31.1, 32.6, 48.7, 51.6, 76.8, 124.0, 124.2, 124.4, 125.7, 125.7, 126.9, 127.3, 128.7, 129.4, 135.8, 137.0, 137.9, 143.1, 145.9, 146.2, 149.3 ppm; HRMS (FAB): *m/z*: calcd for $C_{50}H_{44}O$: 660.3392 [$M^+$]; found: 660.3394. (*Z*)-**1H**: yield=28%; m.p. 98–101°C; $^1$H NMR (500 MHz, $CD_2Cl_2$): $\delta=0.96$–0.98 (m, 3H), 1.39–1.48 (m, 4H), 1.48–1.54 (m, 2H), 1.55–1.56 (m, 2H), 1.70–1.73 (m, 2H), 2.03–2.06 (m, 2H), 3.98 (t, $J=6.8$ Hz, 2H), 5.46 (s, 2H), 5.69 (s, 2H), 6.80 (d, $J=12.1$ Hz, 1H), 6.83–6,91 (m, 17H), 7.11 (d, $J=12.1$ Hz, 1H), 7.31 ppm (d, $J=7.5$ Hz, 4H); $^{13}$C NMR (125 MHz, $CD_2Cl_2$): $\delta=14.5$, 23.3, 27.0, 30.0, 31.1, 32.2, 32.5, 48.8, 51.9, 76.7, 123.7, 124.1, 125.4, 125.7, 125.9, 134.4, 135.9, 137.3, 142.4, 145.8, 146.0, 149.3 ppm. (*E*)-**1OM**: yield=53%; m.p. 254–255°C; $^1$H NMR (500 MHz, $CD_2Cl_2$): $\delta=0.93$–0.97 (m, 3H), 1.22–1.32 (m, 2H), 1.36–1.42 (m, 4H), 1.46–1.56 (m, 4H), 1.67–1.74 (m, 2H), 2.01–2.07 (m, 2H), 3.94–3.96 (m, 8H), 5.73 (s, 2H), 5.76 (s, 2H), 6.55 (t, $J=2.2$ Hz, 1H), 6.64 (d, $J=16.4$ Hz, 1H), 6.89(t, $J=2.2$ Hz, 2H), 6.92–6.96 (m, 8H), 7.30–7.35 (m, 8H), 7.55 ppm (d, $J=16.4$ Hz, 1H); $^{13}$C NMR (125 MHz, $CD_2Cl_2$): $\delta=14.5$, 23.3, 27.0, 30.0, 30.2, 31.1, 32.2, 32.5, 48.7, 51.6, 56.1, 76.7, 100.3, 105.6, 124.0, 124.1, 124.9, 125.7, 125.7, 126.7, 135.8, 136.9, 139.8, 143.1, 145.9, 146.1, 149.4, 161.9 ppm; HRMS (FAB): *m/z*: calcd for $C_{52}H_{48}O_3$: 720.3603 [$M^+$]; found: 720.3602. (*Z*)-**1OM**: yield=26%; m.p. 186–188°C; $^1$H NMR (500 MHz, $CD_2Cl_2$): $\delta=0.97$ (m, 3H), 1.40–1.45 (m, 4H), 1.48–1.50 (m, 4H), 1.69–1.73 (m, 2H), 2.02 (quin, $J=6.8$ Hz, 2H), 2.73 (s, 6H), 3.90 (t, $J=6.8$ Hz, 2H), 5.50 (s, 2H), 5.69 (s, 2H), 5.86 (d, $J=2.3$ Hz, 2H), 5.97 (t, $J=2,3$ Hz, 1H), 6.68 (br, 4H), 6.89 (d, $J=11.8$ Hz, 1H), 6.93 (br, *6*H), 7.04 (d, $J=11.8$ Hz, 1H), 7.30 ppm (br, 6H); $^{13}$C NMR (125 MHz, $CD_2Cl_2$): $\delta=14.5$, 23.3, 27.0, 30.0, 30.2, 31.1, 32.5, 48.8, 51.9, 53.6, 76.6, 101.4, 106.8, 123.3, 123.9, 124.2, 125.4, 126.3, 126.6, 134.7, 136.2, 138.7, 142.5, 145.8, 146.1, 148.9, 160.9 ppm.

**General Heck route for the synthesis of (*E*)-1R ((*E*)-1Pr and (*E*)-1Bu)**: A mixture of **3** (50 mg, 0.08 mmol), $Pd(OAc)_2$ (6 mg, 0.02 mmol), P(*o*-tolyl)$_3$ (12 mg, 0.04 mmol), 3,5-dialkylstyrene (0.24 mmol), anhydrous DMF (1.5 mL), and triethylamine (1.5 mL) was heated to 90°C for 16 h under argon. The mixture was concentrated under reduced pressure, and the residue was dissolved in $CH_2Cl_2$ and washed wish brine. The organic layer was dried over anhydrous $MgSO_4$ and the filtrate was concentrated under reduced pressure. Column chromatography with $CH_2Cl_2$/hexane

  

(v/v = 1:4) as the eluent afforded the product. (*E*)-**1Pr**: yield = 73%; m.p. > 300 °C; $^1$H NMR (500 MHz, $CD_2Cl_2$): $\delta$ = 0.95–0.98 (m, 3H), 1.39–1.41 (m, 14H), 1.45–1.57 (m, 6H), 1.46–1.56 (m, 4H), 1.71 (m, 2H), 2.05 (m, 2H), 3.06 (septet, $J$ = 6.9 Hz, 2H), 3.95 (t, $J$ = 6.8 Hz, 2H), 5.73 (s, 2H), 5.80 (s, 2H), 6.71 (d, $J$ = 16.5 Hz, 1H), 6.93–6.97 (m, 8H), 7.19 (m, 1H), 7.30–7.36 (m, 8H), 7.42 (m, 2H), 7.52–7.55 (m, 2H), 7.54 ppm (d, $J$ = 16.5 Hz, 1H); $^{13}$C NMR (125 MHz, $CD_2Cl_2$): $\delta$ = 14.5, 23.3, 24.5, 27.0, 30.0, 30.2, 31.1, 32.6, 35.0, 48.7, 51.6, 76.7, 123.1, 123.7, 124.0, 124.1, 125.1, 125.6, 125.7, 127.1, 134.7, 137.6, 137.7, 143.1, 145.9, 146.2, 149.2, 150.3 ppm; HRMS (FAB): $m/z$: calcd for $C_{56}H_{56}O$: 744.4331 [$M^+$]; found: 744.4332. (*E*)-**1Bu**: yield = 76%; m.p. > 300 °C; $^1$H NMR (500 MHz, [D$_6$]DMSO): $\delta$ = 0.88–0.91 (m, 3H), 1.31–1.32 (m, 4H), 1.34–1.40 (m, 4H), 1.42 (s, 18H), 1.57–1.60 (m, 2H), 1.92–1.95 (m, 2H), 3.92 (t, $J$ = 6.7 Hz, 2H), 5.76 (s, 2H), 5.87 (s, 2H), 6.61 (d, $J$ = 16.4 Hz, 1H), 6.91–6.95 (m, 8H), 7.37–7.39 (m, 8H), 7.45 (s, 1H), 7.59 (d, $J$ = 1.4 Hz, 2H), 7.70 ppm (d, $J$ = 16.4 Hz, 1H); $^{13}$C NMR (125 MHz, [D$_6$]DMSO): $\delta$ = 14.0, 22.1, 25.6, 28.7, 28.9, 29.7, 31.4, 34.6, 47.3, 50.0, 75.5, 121.0, 123.4, 123.7, 125.0, 126.3, 134.9, 136.0, 137.1, 141.6, 142.1, 145.1, 145.3, 148.1, 150.8 ppm; HRMS (FAB): $m/z$: calcd for $C_{58}H_{60}O$: 772.4644 [$M^+$]; found: 772.4651.

**General procedure for the synthesis of (*Z*)-1Pr and (*Z*)-1Bu**: An $N_2$-purged solution of (*E*)-**1R** in dichloromethane (1 mM) was irradiated with 352 nm in a Rayonet photochemical reactor for 30 min. The solvent was removed under reduced pressure. Preparative HPLC with EA/hexane (v/v = 5:95) as the eluent afforded the product. (*Z*)-**1Pr**: yield = 98%; m.p. > 86–88 °C; $^1$H NMR (500 MHz, [D$_6$]DMSO): $\delta$ = 0.45 (d, $J$ = 6.9 Hz, 12H), 0.89–0.92 (m, 3H), 1.33–1.41 (m, 8H), 1.55 (m, 2H), 1.91–1.94 (m, 2H), 2.24 (septet, $J$ = 6.9 Hz, 2H), 3.89 (t, $J$ = 7.0 Hz, 2H), 5.44 (s, 2H), 5.70 (s, 2H), 6.36 (s, 2H), 6.51–6.52 (m, 3H), 6.56 (m, 2H), 6.79 (m, 2H), 6.85 (d, $J$ = 11.7 Hz, 1H), 6.90–6.91 (m, 4H), 7.13 (d, $J$ = 11.7 Hz, 1H), 7.27–7.28 (m, 2H), 7.33 ppm (m, 4H); $^{13}$C NMR (125 MHz, [D$_6$]DMSO): $\delta$ = 14.0, 22.1, 23.0, 25.7, 28.8, 28.9, 29.7, 31.4, 32.8, 47.4, 50.6, 75.5, 122.7, 123.2, 123.3, 123.6, 123.7, 124.4, 124.4, 124.6, 124.8, 125.7, 134.4, 134.8, 135.8, 141.3, 144.7, 145.1, 145.2, 145.4, 147.7, 147.9 ppm; HRMS (FAB): $m/z$: calcd for $C_{56}H_{56}O$: 744.4331 [$M^+$]; found: 744.4334. (*Z*)-**1Bu**: yield = 99%; m.p. 116–120 °C; $^1$H NMR (500 MHz, [D$_6$]DMSO): $\delta$ = 0.63 (br, 18H), 0.89–0.92 (m, 3H), 1.33–1.45 (m, 8H), 1.54–1.57 (m, 2H), 1.90–1.96 (m, 2H), 3.88 (t, $J$ = 6.9 Hz, 2H), 5.44 (s, 2H), 5.69 (s, 2H), 6.49–6.56 (m, 5H), 6.79 (t, $J$ = 7.2 Hz, 2H), 6.84–6.93 (m, 5H), 7.16 (d, $J$ = 11.8 Hz, 1H), 7.28 (d, $J$ = 7.2 Hz, 2H), 7.31 ppm (m, 3H); $^{13}$C NMR (125 MHz, [D$_6$]DMSO): $\delta$ = 14.0, 22.1, 25.6, 28.7, 28.9, 29.7, 30.5, 31.4, 33.6, 75.4, 120.7, 122.8, 122.9, 123.1, 123.3, 123.6, 124.4, 124.4, 124.4, 124.8, 124.8, 125.7, 134.8, 135.1, 141.3, 144.7, 145.1, 145.2, 145.5, 147.9, 149.5 ppm; HRMS (FAB): $m/z$: calcd for $C_{58}H_{60}O$: 772.4644 [$M^+$]; found: 772.4638.

## Acknowledgements

Financial support for this research was provided by the National Science Council and Academia Sinica of Taiwan, ROC. The computing time granted by the National Center for High-Performance Computing and the Computing Center of Academia Sinica is acknowledged.

[1] a) V. Balzani, A. Credi, F. M. Raymo, J. F. Stoddart, *Angew. Chem.* **2000**, *112*, 3484–3530; *Angew. Chem. Int. Ed.* **2000**, *39*, 3348–3391; b) G. S. Kottas, L. I. Clarke, D. Horinek, J. Michl, *Chem. Rev.* **2005**, *105*, 1281–1376; c) E. R. Kay, D. A. Leigh, F. Zerbetto, *Angew. Chem.* **2007**, *119*, 72–196; *Angew. Chem. Int. Ed.* **2007**, *46*, 72–191.

[2] a) T. R. Kelly, M. C. Bowyer, K. V. Bhaskar, D. Bebbington, A. Garcia, F. Lang, M. H. Kim, M. P. Jette, *J. Am. Chem. Soc.* **1994**, *116*, 3657–3658; b) P. V. Jog, R. E. Brown, D. K. Bates, *J. Org. Chem.* **2003**, *68*, 8240–8243; c) R. Annunziata, M. Benzglia, M. Cinquini, L. Raimondi, F. Cozzi, *J. Phys. Org. Chem.* **2004**, *17*, 749–751; d) I. Alfonso, M. I. Burguete, S. V. Luis, *J. Org. Chem.* **2006**, *71*, 2242–2250; e) K. Nikitin, H. Müller-Bunz, Y. Ortin, M. J. McMlinchey, *Chem. Eur. J.* **2009**, *15*, 1836–1843; f) A. Comotti, S. Bracco, P. Valsesia, M. Beretta, P. Sozzani, *Angew. Chem. Int. Ed.* **2010**, *49*, 1760–1764.

[3] a) H. Iwamura, K. Mislow, *Acc. Chem. Res.* **1988**, *21*, 175–182; b) G. Yamamoto, *Tetrahedron* **1990**, *46*, 2761–2772; c) A. M. Stevens, C. J. Richards, *Tetrahedron Lett.* **1997**, *38*, 7805–7808; d) J. Clayden, J. H. Pink, *Angew. Chem.* **1998**, *110*, 2040–2043; *Angew. Chem. Int. Ed.* **1998**, *37*, 1937–1939; e) L. E. Harrington, L. S. Cahill, M. J. McGlinchey, *Organometallics* **2004**, *23*, 2884–2891; f) I. Eryazici, P. Wang, C. N. Moorefield, M. Panzer, S. Durmus, C. D. Shreiner, G. R. Newkome, *Dalton Trans.* **2007**, 626–628; g) W. Setaka, T. Nirengi, C. Kabuto, M. Kira, *J. Am. Chem. Soc.* **2008**, *130*, 15762–15763.

[4] For light-driven molecular shuttles, see: a) H. Murakami, A. Kawabuchi, R. Matsumoto, T. Ido, N. Nakashima, *J. Am. Chem. Soc.* **2005**, *127*, 15891–15899, and references therein; b) W. Zhou, D. Chen, J. Li, J. Xu, J. Lv, H. Liu, Y. Li, *Org. Lett.* **2007**, *9*, 3929–3932; c) K. Hirose, Y. Shiba, K. Ishibashi, Y. Doi, Y. Tobe, *Chem. Eur. J.* **2008**, *14*, 3427–3433; d) A. Coskun, D. C. Friedman, H. Li, K. Patel, H. A. Khatib, J. F. Stoddart, *J. Am. Chem. Soc.* **2009**, *131*, 2493–2495.

[5] a) J. P. Sestelo, T. R. Kelly, *Appl. Phys. A* **2002**, *75*, 337–343; b) M. F. Hawthorne, J. I. Zink, J. M. Skelton, M. J. Bayer, C. Liu, E. Livshits, R. Baer, D. Neuhauser, *Science* **2004**, *303*, 1849–1851; c) B. L. Feringa, *J. Org. Chem.* **2007**, *72*, 6635–6652; d) M. M. Pollard, M. Lubomska, P. Rudolf, B. L. Feringa, *Angew. Chem.* **2007**, *119*, 1300–1302; *Angew. Chem. Int. Ed.* **2007**, *46*, 1278–1280; e) G. London, G. T. Carroll, T. F. Landaluce, M. M. Pollard, P. Rudolfb, B. L. Feringa, *Chem. Commun.* **2009**, 1712–1714; f) E. M. Geertsema, S. J. van der Molen, M. Martens, B. L. Feringa, *Proc. Natl. Acad. Sci. USA* **2009**, *106*, 16919–16924.

[6] a) J. E. Walker, *Angew. Chem.* **1998**, *110*, 2438–2450; *Angew. Chem. Int. Ed.* **1998**, *37*, 2308–2319; b) R. D. Vale, R. A. Milligan, *Science* **2000**, *288*, 88–95; c) K. Kinbara, T. Aida, *Chem. Rev.* **2005**, *105*, 1377–1400.

[7] B. Champin, P. Mobian, J.-P. Sauvage, *Chem. Soc. Rev.* **2007**, *36*, 358–366.

[8] a) F. M. Raymo, *Angew. Chem.* **2006**, *118*, 5375–5377; *Angew. Chem. Int. Ed.* **2006**, *45*, 5249–5251; b) A. Credi, *Aust. J. Chem.* **2006**, *59*, 157–169; c) S. Saha, J. F. Stoddart, *Chem. Soc. Rev.* **2007**, *36*, 77–92.

[9] J.-S. Yang, Y.-T. Huang, J.-H. Ho, W.-T. Sun, H.-H. Huang, Y.-C. Lin, S.-J. Huang, S.-L. Huang, H.-F. Lu, I. Chao, *Org. Lett.* **2008**, *10*, 2279–2282.

[10] J.-S. Yang, C.-W. Ko, *J. Org. Chem.* **2006**, *71*, 844–847.

[11] V. Diemer, H. Chaumeil, A. Defoin, A. Fort, A. Boeglin, C. Carré, *Eur. J. Org. Chem.* **2006**, 2727–2738.

[12] E. L. Eliel, S. H. Wilen, L. N. Mander, *Stereochemistry of Organic Compounds*, Wiley, New York, **1994**.

[13] *Handbook of Chemistry and Physics* (Ed.: D. R. Lide), CRC Press, Baoca Raton, **1997**.

[14] L. Liu, Q-X. Guo, *Chem. Rev.* **2001**, *101*, 673–695.

[15] Y. Zhao, D. G. Truhlar, *Acc. Chem. Res.* **2008**, *41*, 157–167.

[16] To search for conformers, the following bonds are rotated: the $C_{sp^2}$–$O_{sp^3}$ bond of the methoxy group *para* to the brake in all (*Z*)-**1R**, the $C_{sp^2}$–$C_{sp^3}$ bonds of the substituents (*tert*-butyl and isopropyl) on the brake unit of (*Z*)-**1Pr** and (*Z*)-**1Bu**, and the $C_{sp^2}$–$O_{sp^3}$ bond of the brake unit of (*Z*)-**1OM**. There are two ground-state conformers for (*Z*)-**1H** and (*Z*)-**1NO**, but it increases to eight unique conformers for (*Z*)-**1OM**, (*Z*)-**1Pr**, and (*Z*)-**1Bu**. For the transition state of pentiptycene rotation, there is one conformer for (*Z*)-**1H** and (*Z*)-**1NO** and four conformers for (*Z*)-**1OM**, (*Z*)-**1Pr**, and (*Z*)-**1Bu**. For the brake rotation, there are two transition-state conformers for (*Z*)-**1H**, (*Z*)-**1Bu** and (*Z*)-**1NO**, and eight for (*Z*)-**1OM** and (*Z*)-**1Pr**. In the homodesmotic calculations, there are three unique conformers for *meta*-dimethoxy (*m*-**OM**), *meta*-diisopropyl (*m*-**Pr**), and *meta*-di-*tert*-butyl (*m*-**Bu**) benzenes (with one conformer with a degeneracy of 2), and one conformer for benzene and *meta*-dinitrobenzene (*m*-**NO**). More detailed results and discussion of the DFT calculations will be reported elsewhere.

  

[17] The DFT-optimized structure of (*Z*)-**1NO** and the Mulliken charges obtained at the BMK/6-311+G** level were used for single-point energy evaluation with the Drieding force field. In the ground state, one of the nitro groups was pointing toward the rotor (termed in-nitro) and the other (termed out-nitro) was not. When the atomic charges within the in-nitro group were assigned as zero, the calculated energy was raised by 3.7 kcal mol$^{-1}$.
[18] H. Görner, H. J. Kuhn, *Adv. Photochem.* **1995**, *21*, 1–117.
[19] a) H. Meier, *Angew. Chem.* **1992**, *104*, 1425–1446; *Angew. Chem. Int. Ed. Engl.* **1992**, *31*, 1399–1420; b) P. Klán, J. Wirz, *Photochemistry of Organic Compounds: From Concepts to Practice*, Wiley, New York, **2009**.
[20] a) A. M. Schoevaars, W. Kruizinga, R. W. J. Zijlstra, N. Veldman, A. L. Spek, B. L. Feringa, *J. Org. Chem.* **1997**, *62*, 4943–4948; b) M. K. J. ter Wiel, R. A. van Delden, A. Meetsma, B. L. Feringa, *Org. Biomol. Chem.* **2005**, *3*, 4071–4076; c) M. K. J. ter Wiel, B. L. Feringa, *Tetrahedron* **2009**, *65*, 4332–4339.
[21] M. C. Basheer, Y. Oka, M. Mathews, N. Tamaoki, *Chem. Eur. J.* **2010**, *16*, 3489–3496.
[22] a) J.-S. Yang, J.-L. Yan, *Chem. Commun.* **2008**, 1501–1512; b) J.-S. Yang, J.-L. Yan, Y.-X. Jin, W.-T. Sun, M.-T. Yang, *Org. Lett.* **2009**, *11*, 1429–1432.
[23] J.-S. Yang, K.-L. Liau, C.-M. Wang, C.-Y. Hwang, *J. Am. Chem. Soc.* **2004**, *126*, 12325–12335.
[24] Gaussian 03, Revision D.02, M. J. Frisch, G. W. Trucks, H. B. Schlegel, G. E. Scuseria, M. A. Robb, J. R. Cheeseman, J. A. Montgomery, Jr., T. Vreven, K. N. Kudin, J. C. Burant, J. M. Millam, S. S. Iyengar, J. Tomasi, V. Barone, B. Mennucci, M. Cossi, G. Scalmani, N. Rega, G. A. Petersson, H. Nakatsuji, M. Hada, M. Ehara, K. Toyota, R. Fukuda, J. Hasegawa, M. Ishida, T. Nakajima, Y. Honda, O. Kitao, H. Nakai, M. Klene, X. Li, J. E. Knox, H. P. Hratchian, J. B. Cross, V. Bakken, C. Adamo, J. Jaramillo, R. Gomperts, R. E. Stratmann, O. Yazyev, A. J. Austin, R. Cammi, C. Pomelli, J. W. Ochterski, P. Y. Ayala, K. Morokuma, G. A. Voth, P. Salvador, J. J. Dannenberg, V. G. Zakrzewski, S. Dapprich, A. D. Daniels, M. C. Strain, O. Farkas, D. K. Malick, A. D. Rabuck, K. Raghavachari, J. B. Foresman, J. V. Ortiz, Q. Cui, A. G. Baboul, S. Clifford, J. Cioslowski, B. B. Stefanov, G. Liu, A. Liashenko, P. Piskorz, I. Komaromi, R. L. Martin, D. J. Fox, T. Keith, M. A. Al-Laham, C. Y. Peng, A. Nanayakkara, M. Challacombe, P. M. W. Gill, B. Johnson, W. Chen, M. W. Wong, C. Gonzalez, J. A. Pople, Gaussian, Inc., Wallingford CT, **2004**.
[25] N. A. Bumagin, E. V. Luzikova, *J. Organomet. Chem.* **1997**, *532*, 271–273.
[26] R. Adams, Jr., S. Mackenzie, S. Loewe, *J. Am. Chem. Soc.* **1948**, *70*, 664–668.

Received: March 26, 2010
Published online: September 8, 2010

  